Eur. Phys. J. B **47**, 467–478 (2005)
DOI: 10.1140/epjb/e2005-00353-6

THE EUROPEAN PHYSICAL JOURNAL B

Magnetization reversal via bloch points nucleation in nanowires and dots: a micromagnetic study

H. Niedoba[1,a] and M. Labrune[2]

[1] Laboratoire de Magnétisme et d'Optique de Versailles, CNRS UMR 8634, Université de Versailles, 45 avenue des États-Unis, 78035 Versailles, France
[2] Laboratoire PMTM - CNRS UPR9001, Institut Galilée, Université Paris-13, 93430 Villetaneuse, France

Received 30 November 2004 / Received in final form 25 July 2005
Published online 17 November 2005 – © EDP Sciences, Società Italiana di Fisica, Springer-Verlag 2005

Abstract. Micromagnetic studies of the reversal of stripe domains in elements of different geometries are reported. Various 2D and 3D codes are used in order to allow comparison between an infinite slab, nanowires and dots. Starting from a saturated state the establishment of stripe domains through the sample is first studied. Contrary to the thin film case, the nucleation of this pattern is not uniform and is very different to the geometry of a wire or an isolated dot. Special attention is paid to the reversal of the core of the vortex (the remnants of inner walls between up and down domains) which requires the insertion of point singularities called Bloch points (BP) either at surfaces or created in a pair depending on the length allowed for the stripe in the corresponding element. The magnetization distribution around the core of the various BP is described in detail as well as the key characteristics of their motion. Finally, some experiments are suggested predicting the behaviour of stripe domains under an applied field.

PACS. 75.75.+a Magnetic properties of nanostructures – 07.05.Tp Computer modeling and simulation – 75.60.Ch Domain walls and domain structure

1 Introduction

The study of magnetic configurations in confined geometries is currently stimulating intense practical and theoretical attention. This is the case for Co nanowires exhibiting a stripe domain structure which display spin transport effects with potential as magnetic sensors. On the other hand, dots with perpendicular magnetic anisotropy are of great interest in information storage media and more generally in spin-electronic devices [1]. In all these cases the investigation of the nucleation of domain patterns starting from the saturated state, followed by magnetization reversal in an opposite field associated with hysteresis are topics of basic interest for technical applications as well as of fundamental interest in the theory of ferromagnetism. In this paper, these problems will be treated for three different geometries (see Fig. 1): the case of a thin film, a nanowire and finally a dot, all of them exhibiting a uniaxial perpendicular anisotropy. Micromagnetic simulations are used which prove to be instructive in bridging the gap between theory and experiment. It has been already mentioned (see for example Hubert and Schäfer [2]) that under a critical field or at a critical thickness the magnetization starts to deviate from the uniform saturated state towards the form of sinusoidal stripe domains oriented parallel to the applied field. These critical conditions, as well as the magnetization mode at this nucleation point (also labeled spin reorientation transition point), can be derived analytically from micomagnetic theory [3]. While a uniform nucleation is expected over the entire sample for an infinite thin film, the situation is more complex when the magnetization distribution can not be considered as invariant along the applied field direction. In our case, such invariance is lost along the OZ axis parallel to the applied field direction as shown in Figure 1. In nanowires and dots of finite width L, the magnetization starts to fluctuate near the surface before condensing into stripe domains which are parallel to the applied field. In this case it is obvious that the length of stripes is limited along OZ by the width L. A solution, resulting from numerical computation has been reported in reference [4] for dots of Cobalt. While wires and dots are treated here, a full description of stripe nucleation goes beyond the scope of this paper. In the present study, we focus on the necessity of Bloch point injection and propagation to realize the polarity reversal of the core of the wall separating domains. This is needed for topological reasons when reversing the applied field to reach the opposite saturated state [5]. For stripe domain configurations, there is no continuous transformation of magnetization distribution allowed between the saturated state in positive and negative magnetic fields. On the other hand, the existence

[a] e-mail: halina.niedoba@physique.uvsq.fr

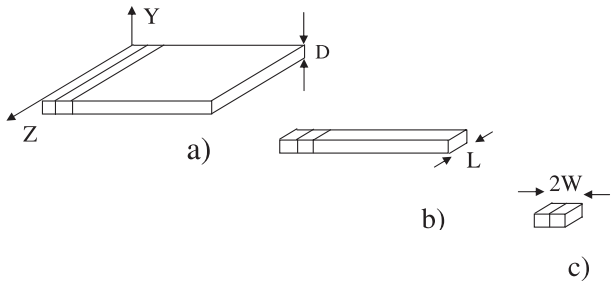

Fig. 1. Different sample geometries analysed: a) infinite thin film, b) infinite wire of width L and c) dot, all elements have the same thickness D. The parallel lines (along OZ) indicate the direction of elongation of the magnetic stripe.

of a continuous magnetization vector field of constant and non-zero length M_S is the basic assumption of micromagnetism. Thus, hysteresis properties may be derived which depend solely on the magnetization distribution and transitions between allowed structures, bearing in mind that any process involving Bloch points is a priori excluded from the computations. However, it has been shown that standard micromagnetic calculations allow the presence of a Bloch point [6–9] which is of course located between mesh points of the discrete calculation. Although the results show strong mesh dependence, they give the right order of magnitude compared to experimental values when reasonable mesh sizes are used, as has been demonstrated in the case of Permalloy thin film disk [8]. The present work takes advantage of the fact that micromagnetic calculations involving Bloch points are technically feasible with a reasonable physical validity, to describe the full hysteresis loop.

This paper is structured as follows. The magnetic parameters and the various geometries considered are described in Section 2. The third part deals with a brief description of the different micromagnetic codes used. A survey of the weak stripe pattern is given in Section 4 which is devoted to the particular case of an infinite thin film. An overview of the magnetization processes near saturation followed by the settlement of stripe domain for dots and nanowires (stripes parallel to the width, L, of the wire) is presented in Section 5 where the remanent state is also discussed. The following Section 6 deals with wire and dot geometries, and describes the switching of the vortex core under a field opposite in direction to that of the wall core magnetization. While in the case of nanowires the periodicity of the magnetic pattern is preserved due to their unlimited length along OX (see Fig. 1b), for dots the magnetic periodicity is lost as the number of stripes is restricted due to their finite size. Bloch point injection and propagation mechanism is studied first for the case of stripe length smaller than the domain width (6.2.1). In Section 6.2.2 the same analysis is performed for the opposite situation where the size of the elements leads to stripe domains longer than one magnetic period. All these results are compared to available experimental data as well as domain observations, and some suggestions for future experiments are included.

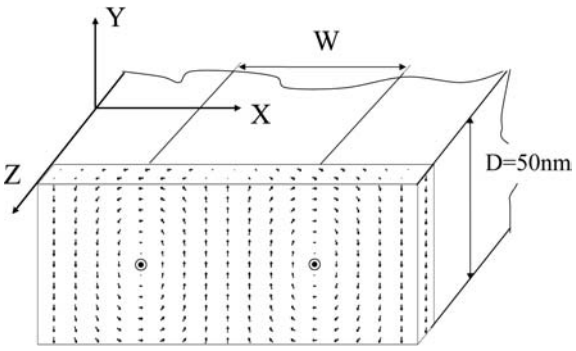

Fig. 2. Equilibrium magnetization profile for a single film 50 nm thick in zero field over one period $2W$ of a stripe domain. The magnetization is independent of the Z coordinate. The lengths of the arrows are proportional to the corresponding in-plane projections of the magnetization moments. The polarity of the inner Bloch walls is stressed: $(+OZ)$ in the present situation.

2 Magnetic parameters and geometry

The first geometry considered corresponds to an infinite thin film $D = 50$ nm thick (Fig. 1a). The magnetic parameters used correspond to typical values for hcp cobalt thin epitaxial films namely, saturation magnetization $M_S = 1400$ kA/m, exchange constant $A = 1.8 \times 10^{-11}$ J/m and uniaxial anisotropy constant $K = 5 \times 10^5$ J/m^3, the easy axis being perpendicular to the film (OY axis). Two magnetic characteristic lengths can be defined, one is the Bloch wall width $\ell_B = \pi\sqrt{A/K} = 19$ nm and the other one the exchange length $\ell_{ex} = \pi\sqrt{A/(\frac{1}{2}\mu_o M_S^2)} = 12$ nm. The quality factor ratio Q defined as the anisotropy field $B_K = 2K/M$ divided by the demagnetising field $B_D = \mu_O M_S$ becomes $Q = K/(\frac{1}{2}\mu_O M_S^2) = 0.4$. It is well known [2,10] that above a critical layer thickness, D_C, a weak stripe pattern is expected of period 2W. The value of this critical layer thickness is: $D_C \approx 2\,\pi\sqrt{A/K} = 2l_B = 38$ nm for very low quality factor and it decreases with increasing Q (more precisely, for $Q = 0.4$, the critical thickness is reduced to two thirds of the previous value: i.e. 25 nm). One period, $2W$, of such a pattern is schematically drawn in Figure 2 for an infinite thin film. Essentially, the magnetic pattern is composed of a succession of up and down magnetized domains with closure domains near the surfaces. Observed by surface sensitive magnetic microscopies such as Kerr or magnetic force microscopy, the patterns look like infinite parallel stripes along the axis parallel to which the saturating field was initially applied (OZ).

The second geometry studied breaks the invariance along OZ while the periodicity of the pattern along OX is preserved. This is the case for an infinite nanowire. Note that we have used the same thickness $D = 50$ nm for all geometries we have studied (Figs. 1a, b and c). The parallel stripes are now limited in length by the width L of the wire. Two cases are considered, firstly the situation with $L < W$ where W is the equilibrium domain width in zero magnetic field; in the present situation with $W = 58$ nm

(see Sect. 6) we chose $L_1 = 40$ nm. Secondly, we studied the situation where $L > 2W$ choosing $L_2 = 200$ nm.

Finally, we considered the case of a single Co dot (Fig. 1c) with thickness D, length $L_{1,2}$ and width equal to $2W$. Therefore, in the remanent state, the dot is expected to be able to support only one magnetic period at equilibrium.

3 Numerical

Depending on the geometry considered, three different calculation codes were used. The (finite-difference) code applied to an infinite thin film was initially designed for the determination of two-dimensional (2D) Néel line structures in garnet epilayers [11] and adapted in order to incorporate the periodical nature of the magnetization pattern [5]. The continuous magnetization distribution is replaced by a set of constant magnetization prisms of infinite length along Z and of square cross section, size a. The parameter a was chosen so that the ratio ℓ_B/a and ℓ_{ex}/a remained larger than ≈5, thus $a = 2$ nm in all calculations. Using the LLG Micromagnetic simulator™ [12] we have modelled the domain structures for the case of the wire geometry (3D problem). One magnetic period of the structure is divided into cubic mesh cells ($a^3 = 2 \times 2 \times 2$ nm^3) while convenient periodic boundary conditions in planes $X = 0$ and $X = 2W$ are ensured. We use this code to solve the Landau-Lifshitz (LL) equation:

$$\frac{d\vec{M}}{dt} = \frac{\gamma}{1+\alpha^2}\vec{M} \times \vec{H}_{eff} - \frac{\gamma\alpha}{(1+\alpha^2)\,M_S}\vec{M} \times [\vec{M} \times \vec{H}_{eff}]$$

where the gyromagnetic factor $\gamma = \mu_O(\frac{-e}{m}) = -2,211 \times 10^5$ (mA^{-1} s^{-1}). The damping (Gilbert) constant α was in most cases taken as $\alpha = 0.5$. Finally, in the case of dots, the numerical calculations were performed with the public micromagnetic program OOMMF [13]. As before, the mesh cells used in the calculations were cubic ($a = 2$ nm) and the same LL equation solved, keeping the value for the Gilbert damping constant unchanged. The convergence criterion for quasistatic equilibrium calculations was $\frac{1}{M_S}\left|\frac{d\vec{M}}{dt}\right| < 0.01$ °/ns at every mesh point. This way of exiting the calculation is quite similar to that used for the LLG Micromagnetic simulator™ where the convergence criterion concerns the absolute value of the largest change in a single direction cosine $(Max - M) < 10^{-6}$.

The calculations show some dependence on mesh size. The critical reversal field increases with decreasing mesh size as will be discussed in the following sections. However, to allow for a clear comparison between the calculations done for different geometries: film, nanowire and dot, the same cell size was used: $a = 2$ nm, which corresponds to $\ell_{ex}/a = 6$. This ratio gives a good order of magnitude of the critical field values compared to that obtained experimentally for cobalt films [14] and is also quite similar to that used by Thiaville et al. to describe the magnetization reversal of Permalloy circular disk [8].

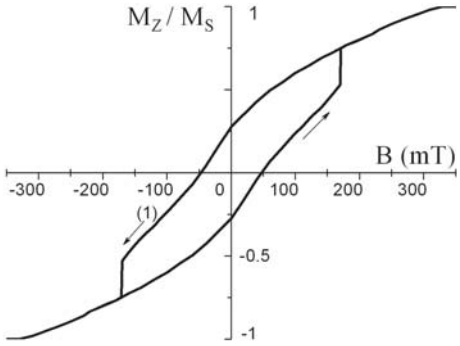

Fig. 3. 2D computed magnetization curve for an infinite thin film (mesh size $a = 2$ nm.).

4 Micromagnetic modelling: case of a thin film

Stripe domains exhibit various configurations ranging from a succession of up and down domains found in high Q materials to stray-field free patterns of the Landau-Lifshitz type in small Q materials. The epitaxial cobalt films studied here, with $Q = 0.4$ correspond to the latter situation. Figure 2 exhibits the equilibrium magnetization profile for the single film 50 nm thick in zero field, after demagnetizing from saturation along $+OZ$. One can observe in this figure closure areas in the vicinity of the top and bottom surfaces which ensure a virtually stray-field free magnetization configuration with alternate flux circulations. In other words, the magnetization pattern can be viewed as a row of vortices, where, in the core of all of them the magnetization always points in the same direction: +OZ. As the magnetic period $2W$ is an additional variable in the minimization process, the configuration of lowest energy provides the equilibrium domain period and the associated magnetization distribution. The numerical calculations of the equilibrium magnetization are repeated for each value of an applied field in order to simulate hysteresis loops. The same field orientation, namely an in-plane longitudinal field (along OZ) is kept throughout the whole paper. The hysteresis loop of the infinite thin film is shown in Figure 3. This curve is in reasonable agreement with the experimental ones obtained for thin Co films of equivalent thickness [14]. The characteristic shape of the B(M) curve may be explained as followed. Upon decreasing the magnetic field starting from in-plane saturation ($+OZ$), the magnetization progressively tilts out of the plane in alternate directions and then transforms into stripes separated in the mid-plane by simple Bloch wall segments while closure domains near both surfaces ensure a nearly stray-field free pattern. Note that the Bloch walls are initially polarized parallel to the applied field ($+OZ$) and contribute to non zero magnetization in the remanent state. Conversely, the zero-field pattern obtained starting from the opposite saturation state ($-OZ$) will lead to Bloch wall segments of opposite polarisation. When the magnetic field is further decreased and then reversed (path 1 in Fig. 3), the wall shrinks while closure domains extend. Finally, the inner Bloch segments

are transformed in circular Bloch lines whose position coincides with the vortex cores already visible in Figure 2, magnetized opposite to the applied field. The reversal of the vortex core occurs for $B = -171$ mT and gives rise to the large jump of magnetization observed in the hysteresis loop. Refining the mesh results only in changes of the core reversal field but does not affect either the remanent magnetization or the saturation field. The general tendency is for the switching field to increase as the mesh size is reduced (e.g. for $a = 2.5$ nm $B = -130$ mT; $a = 2$ nm $B = -171$ mT). Furthermore, in this 2D simulation, the core reversal occurs at the same time over the whole infinite length of each Bloch line. As already mentioned in reference [5], Figure 16, the magnetization reversal may be helped (partly in the present case) by the field-induced magnetization rotation in closure domains which triggers the generation of new Bloch lines, situated at both sides of the initial Bloch line. As these new lines are magnetized parallel to the field, the final reversal may be viewed via the collapse of these various lines. A general description of the vortex core reversal under an applied field, also labelled "topological hysteresis", can be found in the literature; see for example in references [5] and [15].

Figure 4 shows the corresponding evolution of the equilibrium stripe width W as a function of the applied field. The expected domain width is strongly field-dependent in agreement with previous calculations [16,17]. Starting from saturation, the domain width W should increases under a decreasing field till the magnetization reversal occurs. This behaviour can be understood in a crude model where the pattern is assumed to be composed of a succession of domains uniformly magnetized along $\pm\theta$ with $M_Z/M_S = \cos\theta \; BM_S/2K$, separated by thin (Bloch) walls with a magnetization rotation 2θ less than 180°. In this model, the domain period results from a balance between domain anisotropy and demagnetizing energy both of which scale like $\sin^2\theta$, and the associated wall energy, proportional to $(\sin\theta - \theta\cdot\cos\theta)$ [2]. Therefore domain width should be proportional to $W \approx \sqrt{\frac{D\gamma_{180}}{2K}\frac{\sin\theta - \theta\cos\theta}{\sin^2\theta}}$ where γ_{180} is the conventional 180° Bloch wall energy. Starting from positive saturation ($+OZ$), with decreasing field, θ should increase and consequently W should too (see path 1 in Fig. 4). Finally, the large step of the stripe period observed in the reversed field (Fig. 4) corresponds to the jump of magnetization in Figure 3 described previously.

In the literature, controversial results have been published to date. In the experiments reported in [16–19], neither the monotonous variation of W with B [16–18] nor the predicted jumps of the magnetic period of the pattern at the magnetization reversal [19] have been observed. On the other hand, for iron (111) thin films, Foss et al. [20] did report a variation of the period of the stripe with B. However, keeping W constant, one gets a corresponding hysteresis loop for the film quite similar to that of Figure 3. Consequently, in the following calculations for nanowires (Sects. 5 and 6) the domain width will not be adjusted with the applied field amplitude but kept constant as $W(B = 0) = 58$ nm.

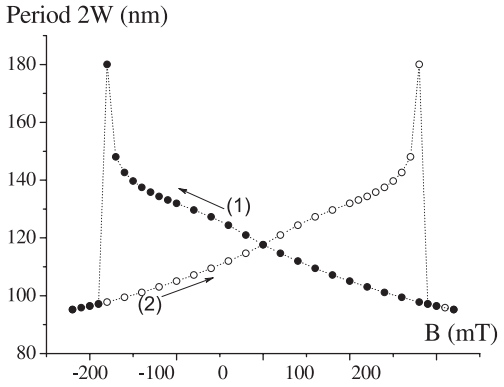

Fig. 4. Variation of the equilibrium magnetic period $2W$ versus the applied field along the hysteresis loop, case of an infinite thin film with mesh size $a = 2$ nm (see text).

5 Nanowires and dots: general overview

5.1 Hysteresis loops

We investigate first the magnetization processes of nanowires of Co (same magnetic parameters as before) with thickness $D = 50$ nm (Fig. 1b). The calculation is restricted to the case of a periodic transverse magnetic pattern of length L along OZ (the external magnetic field is always applied parallel to this direction). A fixed period $2W$ is considered equal to that obtained for the infinite slab in zero field ($2W = 116$ nm). Two situations are reviewed: (i) where the width of the nanowire L_1 is smaller than the domain width itself, in which case we use $L_1 = 40$ nm and (ii) where the width L_2 is larger than one period of the pattern then $L_2 = 200$ nm. We study next small dots (Fig. 1c) of width either L_1 or L_2 and limited in size along OX to 116 nm in which case the magnetic pattern is only constrained by the geometry. In other words, unlike the case of nanowires, we do not impose any periodicity for the magnetic structure. Figure 5 shows the computed hysteresis loops for nanowires and dots. The main characteristic fields (saturation, coercivity and magnetization reversal) are deduced from these plots and gathered in Table 1. As the stripe length L increases, the remanent magnetization value increases too, reaching a maximum for the infinite thin film case. The opposite variation with L is observed for the saturation field which decreases for increasing L. This last effect may be attributed to a demagnetizing shape effect. The saturation field is much lower than the anisotropy field $2K/M$(714 mT) for the infinite slab, however, it increases with the ratio $2W/L$ but is still lower than $2K/M + \mu_o M (= 2474$ mT) even for $L_2 = 40$ nm.

5.2 From saturation to stripe formation

This section is devoted to stripe formation while decreasing the magnetic field starting from saturation. Stripe nucleation is quite a complex process which depends on many factors, therefore the same procedure has been utilized for

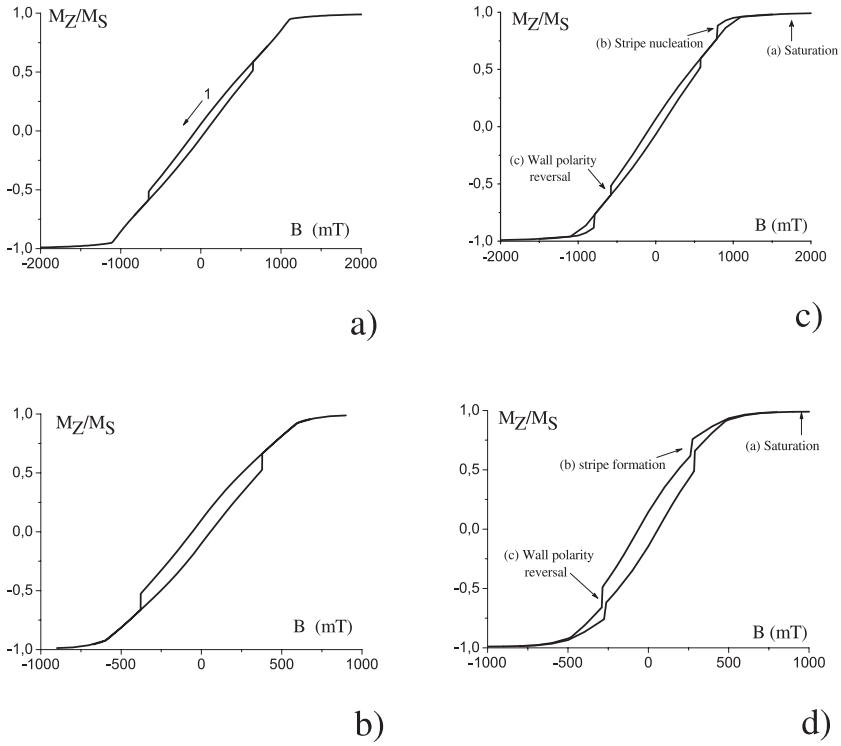

Fig. 5. Hysteresis loops of infinite nanowire of thickness 50 nm and width a) 40 nm and b) 200 nm. Corresponding loops for dots of same thickness 50 nm, equal length 116 nm and width c) 40 nm and d) 200 nm (see text).

Table 1. Key magnetic parameters and different critical fields (mT) for the three different geometries studied.

	$L_1 = 40$ nm		$L_2 = 200$ nm		$L_3 \approx \infty$
Fields (mT)	*Ribbon*	Dot	*Ribbon*	Dot	*Thin film*
Saturation	≈2100	≈2100	≈1200	≈1200	320
Coercivity	64	64	57.5	62	47
magnetization reversal	−651	−577	−379	−290	−171
remanent magnetization (Mz/Ms)	0.058	0.067	0.100	0.144	0.276

all calculations. Starting from saturation (the original initial configuration), the applied field is decreased step by step. At each step, the micromagnetic structure is allowed to relax to its new equilibrium configuration. This last configuration serves as new initial configuration in the next step. For the wire geometries, this part of the loop is described with very small jumps of the applied field equal to $\Delta B = 10$ mT each while larger ones: $\Delta B = 100$ mT are used for the dots. In both cases, stripe nucleation can be associated with a sudden change in the slope of the hysteresis curve (Fig. 5). The change is more pronounced in the case of the dot geometry where stripe nucleation (points (b) in Figs. 5c and 5d) is at the origin of small secondary hysteresis loops whose size is mainly due to the larger ΔB in the dot case. Effectively, the lower the ΔB value, the smaller the secondary hysteresis loop is for either of the two geometries studied. Continuing along the hysteresis curve, the core (or wall polarity) reversal of the stripe pattern occurs in a reverse field, at point (c), before the opposite saturation state finally occurs. As can be seen in Figure 5, all hysteresis curves include the central loop resulting from this wall polarity reversal which will be described in detail in the next section.

In the case of dots with $\Delta B = 100$ mT, the stripe nucleation occurs via a process already described in [4]. In the peculiar case of a wire, where the loop is described with a small jump of field, the development of stripe domains is qualitatively described in Figure 6 for one specific period, $2W$, of the magnetic pattern. Starting from the saturated state, a magnetization distribution similar to that of the well known "Flower" state [21], appears first in a transverse XOY plane (Fig. 6a). It is noticeable that at this stage the transverse M_X component is next to zero and that the magnetization distribution does not depend on the X coordinate so that no periodic structure is generated. Reduction of the field breaks this invariance (Fig. 6b) and a periodicity along OX is settled which gives rise to a very small kink in the hysteresis curve. In successive transverse planes (the YOZ plane) the average magnetization points alternate towards $+/-OY$, and the magnetization distribution observed in these planes may be compared to that of a "S" state occurring in rectangular particle. A further decrease of the field leads to the pattern depicted in Figure 6c with domains alternately pointing up and down as we move along the wire elongation direction. In one domain, and at a given X (Fig. 6c), the distribution is reminiscent of the so-called "leaf" state [22]. Following the evolution of the pattern in the XOY plane while moving along OZ (from the back to the front of the wire) it is

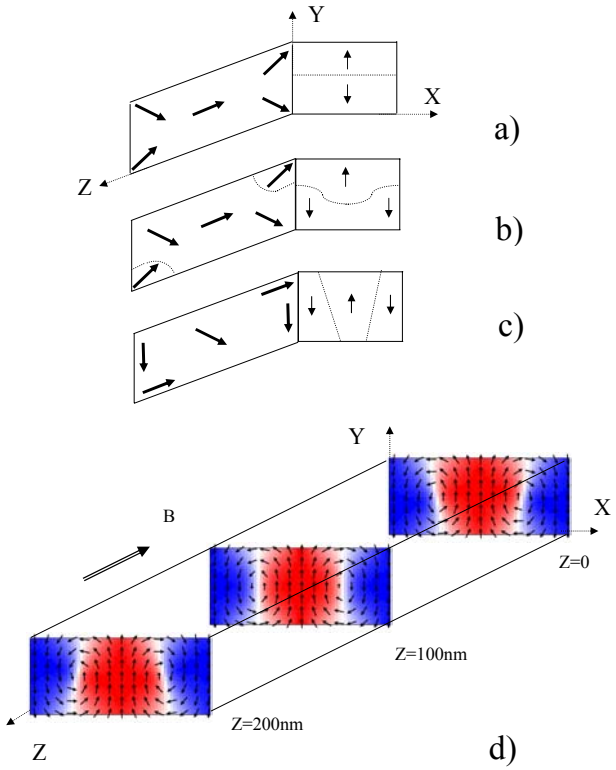

Fig. 6. Illustration of the development of stripe domains in a wire ($L_2 = 200$ nm) in decreasing field from a) to c). At each step, the magnetization distribution is shown in projection on two orthogonal planes: $x = 0$ and $z = 0$. In d) magnetization is shown for three different OXY planes (z = cte), obtained from numerical simulation and corresponding to the situation described in c).

interesting to observe as shown in Figures 6c and 6d that one inner 180° vertical wall cants in the opposite direction as it approaches the head and/or back of the wire.

These complex nucleation mechanisms for nanowires and dots are considerably different from the predicted by a 2D model.

5.3 Remanent state

Finally, in the remanent state, whatever the length L is, one obtains regular parallel stripes oriented along OZ both in the case of nanowires and the dots in contrast to what is quoted in [23] for much larger dots. The remanent domain structures in Co nanowires have also been studied in great detail by Prejbeanu and al. [24] using MFM observations and by Brückner et al. [25] by Lorentz microscopy and micromagnetic simulations. The MFM observations in [24] may be understood in the light of our numerical results (Fig. 7b) where only a partial flux closure is expected near the top and bottom surfaces of the wire leading to non-zero stray fields outside the sample and at the origin of the strong white and black contrast which they observed. Our results are also in qualitative agreement with those of [25] and compatible with the

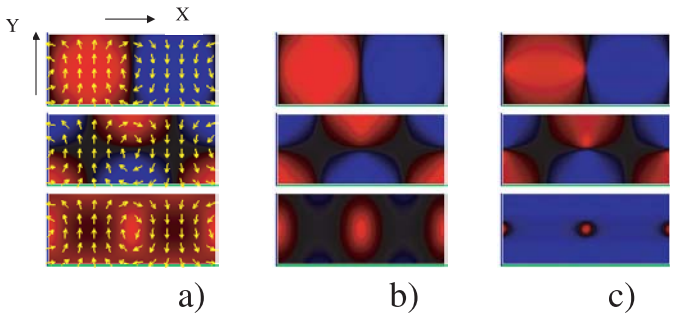

Fig. 7. Maps of magnetization components My (top), Mx (middle) and Mz (bottom) in the XOY plane at the center of the stripes ($z = 100$ nm) in decreasing magnetic field: a) 200 mT, b) 0 mT and c) 370 mT. For each Mx, My and Mz figure, the colours indicate the orientation of the magnetization with respect to the OX, OY and OZ axis respectively: red (white) for parallel and blue (black) for antiparallel orientation.

Lorentz images they obtained. However, as mentioned before, our magnetic pattern is not invariant along Z, and a very small canting (opposite from one face to the other) of the inner 180° walls is still present. Nevertheless, we have averaged the field vector $\vec{\nabla} \times \vec{M}$ over X (direction of the incident electrons). This gives, to first order, an idea of the expected Lorentz contrast in agreement with what is experimentally observed for the inner 180° walls while the imaging of the closure domains is not well elucidated in this approach.

6 Wall polarity reversal for geometries where the stripe length is limited

The evolution of a domain pattern nucleated in a positive ($+OZ$) magnetic field under application of a decreasing field in a wire 200 nm long is shown Figure 7. The magnetization direction in domains and closure areas tends to align with the field direction inducing a shortening of the inner Bloch wall segment as can be seen in Figures 7a and 7b. As already described for an infinite layer, the Bloch wall segment reduces progressively to a Bloch line similar to a vortex (Fig. 7c) in the core of which, due to the exchange constraint, the magnetization is pinned to ($+OZ$) corresponding to the initial saturated state. Therefore almost all the 3D space directions for the magnetization vector $\vec{M}$ are used. According to the Feldkeller representation [26], the unit sphere is nearly covered once leading to a winding magnetization distribution. In such situation, there is no continuous way to reach the opposite saturated state where all the moments will be along $-OZ$. The Bloch line core reversal will not occur suddenly over all the sample as in the 2D problem discussed in Section 4 but will process non-uniformly along the various lines through the propagation of point defects (Bloch points described in the next paragraph) once they are nucleated at a sufficiently high reverse field.

6.1 Bloch points

In micromagnetism, one usually assumes that the magnetization vector $\vec{m}(\vec{r})$ varies continuously with position $\vec{r}$. As shown in the previous paragraph, the present configuration topologically demands the introduction of singularities called Bloch points [26] to reach the saturated state. The definition of a Bloch point implies that the magnitude of the gradient of $\vec{M}(\vec{r})$ tends to infinity in its neighbourhood. It implies that locally the exchange energy density dominates all other energy terms. One can also say that for any closed surface surrounding the point, the magnetization vector covers the unit sphere exactly once [8]. Furthermore, considering all continuous transformations, the Bloch point is the only stable singularity in magnetism [27]. Consequently Bloch-point injection occurs either individually from the surface of the magnetic sample or in pairs in the bulk sample [28]. A good description of the various Bloch-point (BP) configurations such as divergent, convergent, circulating and contra-circulating for example may be found in [29]. The divergent and convergent Bloch points are a well-known basic pair of spherically symmetric solutions given by $\vec{M} = \pm M_s \frac{\vec{r}}{r}$ (with +/– for divergent (+) / convergent (–) BP located at $r = 0$ in spherical coordinates). These BP configurations are also named: "hedgehog" BP. If Cartesian coordinates are used, the previous magnetization distribution may be written as

$$\vec{M} = \pm \frac{M_s}{r} \begin{pmatrix} 1 & 0 & 0 \\ 0 & 1 & 0 \\ 0 & 0 & 1 \end{pmatrix} \begin{pmatrix} x \\ y \\ z \end{pmatrix} \quad (1)$$

the Bloch point being centred at $x = y = z = 0$. An infinite set of distinct Bloch-point configurations exists, as those obtained for example by a θ rotation of the magnetic moments around the Z axis. Their distribution reads:

$$\vec{M} = \pm \frac{M_s}{r} \begin{pmatrix} \cos\theta & -\sin\theta & 0 \\ \sin\theta & \cos\theta & 0 \\ 0 & 0 & 1 \end{pmatrix} \begin{pmatrix} x \\ y \\ z \end{pmatrix} \quad (2)$$

which will be very helpful in the following discussion.

6.2 Bloch-point injection and propagation mechanism

6.2.1 Nanowire and dot with $L_1 = 40$ nm

The reversal of wall polarity or, equivalently, the magnetization switching of the vortex is investigated first for the short stripe case: dot and wire of width $L_1 = 40$ nm. This process begins via the injection of a single Bloch-point per wall. Usually, the beginning of the core reversal for the dot ($119 \times 50 \times 40$ nm^3) is similar to that of a nanowire.

The magnetization distribution in the XOZ plane for $Y = 25$ nm corresponding to half the thickness of the sample, just before the Bloch points are nucleated, is schematically presented in Fig. 8a) over one magnetic period. The two vortex cores shown are still oriented parallel to $+OZ$ but, due to a sudden increase of the magnetic field, the precession, which breaks the symmetry between the two surfaces, has induced an asymmetric variation of the radial magnetization components at their extremities. As mentioned in [8], the increase of the radial components helps the Bloch points to enter through a different surface for each one of the two vortex cores: $z = 0$ nm for the right one and $z = 40$ nm for the left one (Fig. 8b). The field values at which this Bloch points nucleation occurs are $B = -577$ mT and –651 mT for the dot and nanowire respectively. The expected structure of the Bloch-points in zero field is z-circulating convergent on one vortex and z-circulating divergent on the other one according to Slonczewski's description [29]. Figure 8c gives a schematic drawing on an enlarged scale of the nearly-180° wall between two main domains I and II in the CD area. The precession motion in points C and D helps in nucleating the Bloch-point which may be viewed as a result of gathering the two extremities of the wall near the rear sample surface in Figure 8d. In the vicinity of this surface, the magnetization direction of the vortex core is now reversed and lies parallel to the applied field. Obviously, the pattern drawn in Figure 8d is not invariant along OY and the flux should be closed from domain I mainly magnetized along OY to domain II magnetized along $(-OY)$. Figure 9 displays various two-dimensional spatial distributions of the three-dimensional magnetization vector field obtained in the case of a wire (LLG Micromagnetic simulator). The first one is drawn in the XOZ plane at a depth $y = 25$ nm (Fig. 9a), and the second one in the XOY plane perpendicular to the direction of elongation of the stripe (Fig. 9b). There is one arrow per square mesh cell 2×2 nm^2, whose length is proportional to the in-plane magnetization component. The Bloch-point is roughly 8 nm from the surface where it nucleates. As nucleation occurs under the application of a strong external field, the magnetization distribution near the singularity is affected. It is instructive to compare the BP core structure obtained by simulation to that obtained starting from an original divergent BP submitted to a rotation around OZ by an angle θ such that $-\pi/2 < \theta < -\pi$ (a visual inspection of Fig. 9b) shows that θ is of the order of $-3\pi/4$). Calculation of the divergence of the vector field given by equation (2) with $\theta = -3\pi/4$ indicates that this quantity is negative everywhere around the core. However, the simulated structure of the BP is much more complex that this simple picture and the predicted distribution given by equation (2) is only valid in the vicinity of the core of the BP. At a larger scale the flux-closure or vortex pattern along OZ imposes a slight modification of this distribution inducing opposite charges in the core surrounding what is confirmed when using the specific application "divergence" supplied by the OOMMF program.

A large decrease of the exchange energy of the whole magnetic pattern is noticed at the beginning of the vortex core reversal. We propose to give a rough estimation of the nucleation field (see Tab. 1) by comparing mainly the exchange contribution to the energy of a Bloch point to that of the central part of the wall or vortex line. Although the energy density diverges near the center of a Bloch point,

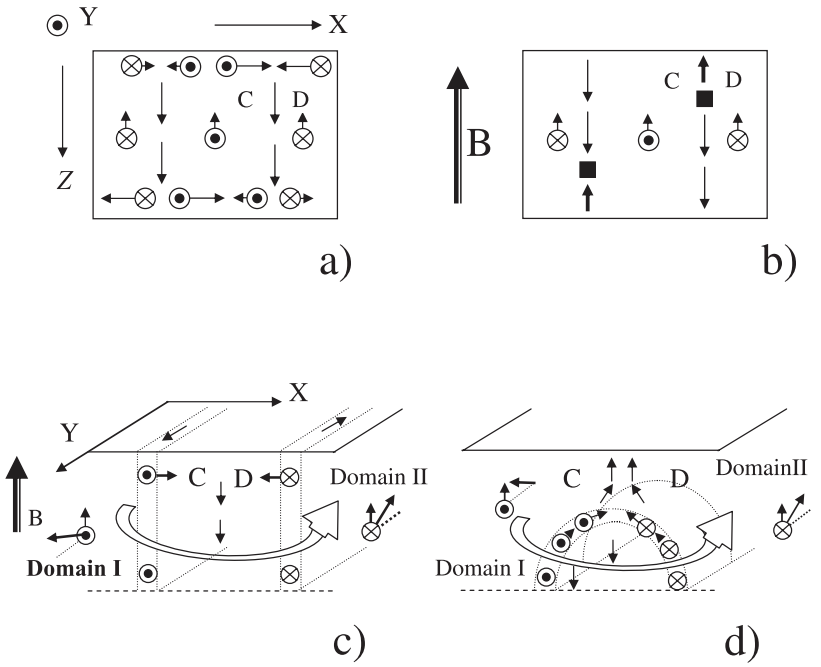

Fig. 8. Top view of the magnetization distribution in the mid-plane of the sample and over one period exhibiting schematically the area where Bloch points are expecting to nucleated. a) Due to core magnetization and next to surfaces, the magnetization of the domain in the vicinity is radialy tilted in order to close the flux. b) Precession effects strengthen these radial components in CD and symmetrically at the bottom of the left wall. Conversely, the radial components decrease at the two other extremities. The same sequence as in a), b) is reproduced from a different perspective in c) before nucleation and d) gives a schematic drawing of the Bloch point magnetization distribution in the vicinity of its core.

it has been shown that the total exchange energy of a finite region of radius R amounts to $E_B = 8\pi\, AR$ [26]. This term is irrelevant to any possible rotation of the magnetization distribution described previously while the next term in energy is the demagnetizing energy which is minimized by this rotation. Therefore, we shall consider E_B in the following. On the other hand, the corresponding exchange contribution of a vortex of length L_1may be taken to be equal to $E_L = 4\pi AL_1$ [27]. It is to be noticed that this equilibrium energy is independent of the diameter of the vortex. Under an applied field B and far from the core of the vortex the magnetization in the domains rotates by a small angle $\delta\theta$ which can be approximated by $\delta\theta \approx$ in $(\delta\theta) = MB/2K$, following the classical Stoner-Wholfarth rotation model. Therefore, an increase of the exchange contribution of the vortex line of the order of $\delta E_L = \mathrm{A} \cdot (\pi^2 \delta\theta) L_1$ is expected. If we take a Bloch point radius of $R = 6$ nm (1/3 of the domain-wall width ℓ_B) the excess of exchange contribution along the line will exceed the energy of a Bloch point for an applied field larger than $B \approx 16KR/\pi ML_1$ which gives: $\left|\vec{B}\right| = 280$ mT. While lower than the computed value, this crude model gives a good order of magnitude of the critical reversal field and predicts that this field must decrease when the width L of the sample increases in agreement with results of our calculations reported in Table 1. Finally, once the nucleation has occurred, the Bloch point propagates along the vortex line ensuring the magnetization reversal of its core.

To investigate the Bloch-point propagation, the time dependent calculations were performed starting with an initial pattern corresponding to the equilibrium magnetization distribution obtained for an applied field value slightly lower (by 1 mT) than the critical reversal field value. At time $t = 0$, an increase of the applied field by a step ΔB was applied to this initial pattern. As the behaviour of the two vortex lines per magnetic period for the nanowire or the full dot is highly symmetrical (e.g. identical BP velocity values, except the opposite direction of motion), only results pertaining to one of them are reported in the following. The reversal process (under the OOMMF program), as already quoted in [8], is associated with a large increase of the maximum torque $(d\vec{M}/dt)$ followed by torque oscillations which can be more or less correlated to the BP crossing successive mesh points, while a large peak signal is noticed at their annihilation. LLG micromagnetic simulations using the evolution of the largest change in a single direction cosine with time applied to the wire geometry gives the same information. In order to quantify the Bloch point motion, its time dependent position was followed visually on a two-dimensional spatial distribution of the magnetization vector display for different cross-sections like that shown in Figure 9.

First off all we extracted the time needed to observe the appearance of the first individual Bloch point on the vortex line: t_1. Once the nucleation is achieved, the Bloch point propagates along the vortex line ensuring the

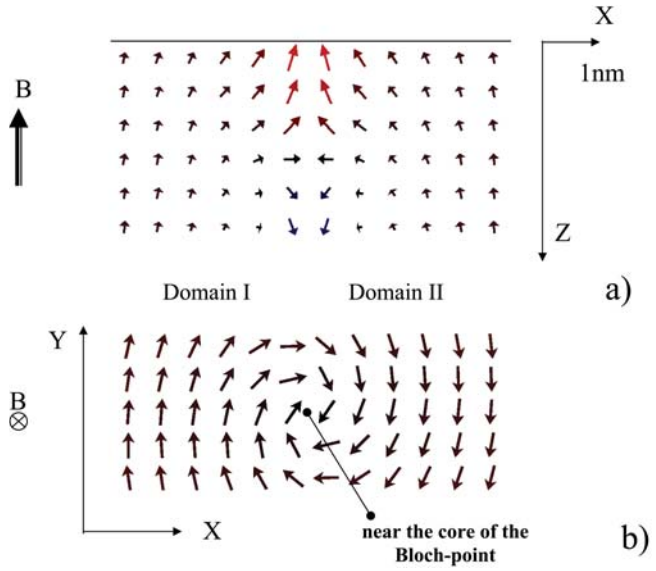

Fig. 9. Enlargement of the magnetization distribution around a Bloch-point obtained by numerical simulation (LLG Micromagnetic simulator) in cross-section a) XOZ plane at mid thickness $y = 25$ nm and b) in a plane perpendicular to the direction of elongation of the stripe: $z = 9$ nm, the case of a nanowire of width $L_1 = 40$ nm. The length of the arrows is proportional to the in-plane component. There is one arrow for each mesh 2 nm × 2 nm.

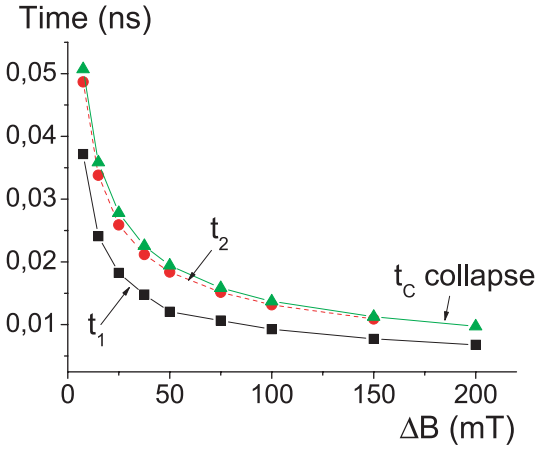

Fig. 10. Variation of the time t_1 (in ns) needed for the appearance of the Bloch point at one surface of the dot ($116 \times D = 50 \times L_1 = 40$ nm^3) versus the increment of field ΔB (mT). t_2 corresponds to the nucleation of a second Bloch point at the other surface of the dot while t_C is the collapse time of the two Bloch points inside the dot.

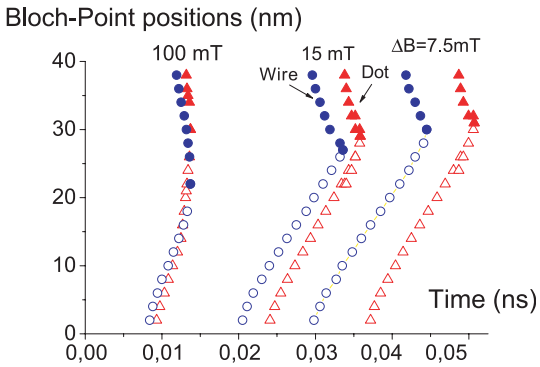

Fig. 11. Evolution with time of the Bloch-point position along the line in the case of the dot with $L_1 = 40$ nm (△ first nucleated point starting from surface $z = 0$ nm and ▲ second Bloch point from the surface $z = 40$ nm) and corresponding points (first ◯ and second ● Bloch-points) for the wire geometry.

magnetization reversal of its core. In most cases studied, a second Bloch point appears with some time delay, at time t_2, at the opposite end of the same line. Finally, both Bloch points collapse at time t_C. These results are gathered in Figure 10 for the peculiar case of the dot and for various values of ΔB ranging from 7.5 mT to 200 mT. The time needed for the appearance of the first Bloch point gets shorter when increasing the amplitude of the field jump ΔB and approximately follows the form: $t_1 \approx 0.1/\sqrt{\Delta B}$, where t_1 is expressed in ns and ΔB in mT. Similar results for the nanowire lead to the relation $t_1 \approx 0.08/\sqrt{\Delta B}$. For a given increment of field, the process always starts first for the nanowire. However, the role of both defects and thermal agitation should not be forgotten.

The positions of the Bloch points during the core reversal are reported in Figure 11 for three different ΔB values only for the sake of clarity. The average Bloch point velocity V_{BP} based on all numerical results shows a quasi-linear dependence versus the field increment and can be expressed as $V_{BP} = v_o + \mu \Delta B$. The BP mobility μ seems slightly higher for the wire case where $\mu = 4.1 \times 10^{-2}$ km s^{-1} mT^{-1} with respect to the dot case where $\mu = 3.7 \times 10^{-2}$ km s^{-1} mT^{-1} while v_o is the order of 1.5 km/s in both cases. Moreover, one can notice that the velocity extrapolates to a nonzero value: v_o for $\Delta B = 0$. Effectively, for $\Delta B < 0$ the core reversal can be obtained by artificially injecting the structure of a BP core in the magnetization configuration located at one end of the vortex line in the initial step of the calculation. Under such conditions, the simulations done in the case of a dot showed that the mobility of the Bloch point is significantly lowered: $\mu = 2.5 \times 10^{-3}$ km s^{-1} mT^{-1} (Fig. 12) while this singularity must travel over the whole length L_1 as no other point injection occurs during the magnetization reversal process. Note that the velocity equals zero for $\Delta B = -580$ mT which corresponds to a zero applied field (keeping in mind that the critical field found for magnetization reversal is $B = -577$ mT). It turns out that it is possible to stabilize, at least for the dot geometry, the two vortex lines containing one Bloch point each, in zero applied field.

A new estimation of the upper limit of the width of the vortex core at reversal can be made based on the above results. For a very weak value: $\Delta B = 1$ mT and assuming that the variation of the longitudinal component of magnetization is mainly due to the polarity reversal of the core of the two vortices one gets an effective radius equal to: $R_{eff} = 5$ nm [with $2L_1(\pi\ R_{eff}^2)2M_S = (M_{Zf} - M_{Zi}).V$; where V corresponds to the volume of the dot and M_{Zf},

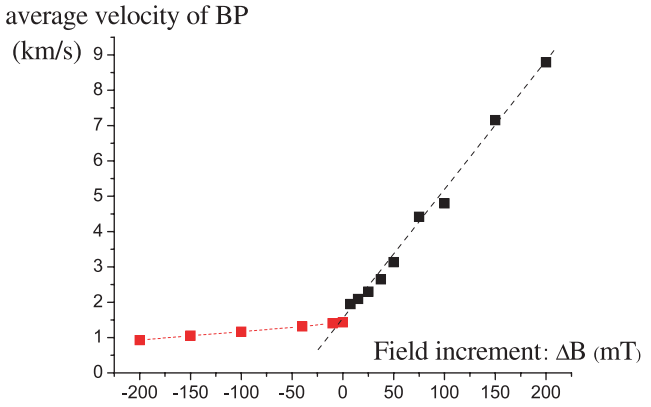

Fig. 12. Case of a dot with $L_1 = 40$ nm. Average velocity of the first Bloch point versus the increment of field ΔB in mT with respect to the critical field ($B = -577$ mT) needed for the spontaneous appearance of a magnetic singularity. The applied field is equal to $B = -(577 + \Delta B)$ mT.

M_{Zi} are the final and initial average value of M_Z over V respectively].

For sake of completeness, the vortex core reversal has also been computed for different values of the damping constant. In the case of lower values but still not too weak (i.e. $\alpha \approx 0.1$) the features are very similar except for the delay before the core reversal starts which increases. For a still lower damping constant ($\alpha \approx 0.01$) an irregular reversal process with the creation of an additional pair of Bloch-points leading to a non-reversed isolated island along the vortex core is observed. A full analysis of the behavior of these isolated islands, also called magnetic drops, can be found in [9]. Finally, the critical fields needed for Bloch-point nucleation always increase upon mesh refinement.

6.2.2 Nanowire and dot with $L_2 = 200$ nm

An increase of the length of the magnetic stripes (always elongated along OZ) due to an enlargement of the dimension of the dot (now $119 \times 50 \times L_2 = 200$ nm) and/or of the lateral width of the wire generates a new mechanism for the vortex core reversal. Under the action of a reverse applied field the core of the walls (lines) are more and more compressed leading to the creation of a pair of Bloch-points in the center of each line at $B = -290$ mT (-379 mT) for dot (and wire) respectively. To understand this phenomenon, it is interesting to estimate the vortex width (or diameter) along the line. Taking the case of a dot as an example, the width of the Bloch-wall segment was estimated in the remanent state. This width labelled ℓ was deduced from the magnetization profile $M_Y(x)$ in the mid-plane of the dot from the slope (dM_Y/dx) for x taken in the middle of the wall. The obtained value, $\ell = 11$ nm, is comparable to what is expected for a pure Bloch wall ($2\sqrt{A/K} = 12$ nm). However, this width decreases when the vortex line reaches the surfaces where $\ell = 8.5$ nm. In a reverse field, just before the nucleation of a pair of Bloch-points, the vortex core diameter gets smaller in the center of the vortex line and one gets $\ell = 5.1$ nm in the middle of the dot while $\ell = 6.4$ nm at the vortex extremities which explains that the Bloch-points are no longer nucleated at the line borders. Once the pair of Bloch-points is nucleated, they move towards the nearest surface in order to reverse the wall chirality. In addition, for very high value of the reversal field (large ΔB) an isolated BP may nucleate from one surface.

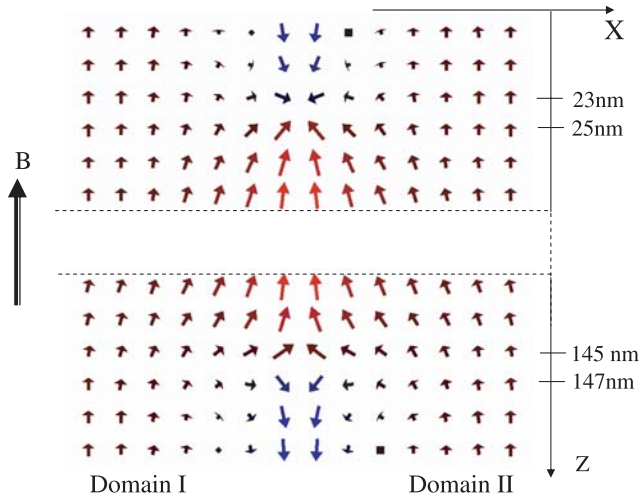

Fig. 13. Top view in the plane $y = 25$ nm of the magnetization distribution showing the presence of a pair of Bloch-points located at $z = 24$ nm and 146 nm. Case of a nanowire 50 nm thick, of width $L_2 = 200$ nm under an applied field $B = -(378 + 50)$ mT at time $t = 0.03$ ns.

Figure 13 gives a top view (plane $y = 25$ nm) of the magnetization distribution for the wire geometry showing the intimate structure of the pair of Bloch-points. The structure of the second one located at $z \approx 146$ nm is similar to that already described in the previous section. Around the first BP (at $z \approx 24$ nm), the magnetization distribution can be crudely described by equation (2) in the case of a convergent point with $0 < \theta < \pi/2$. A visual inspection leads to a rotation angle roughly equal to $\theta \approx +\pi/4$. The magnetic charges are positive in the vicinity of both points, the charge density being higher for the first Bloch point than for the second one. This is clearly visible in Figure 13 where near $z = 24$ nm, the BP structure is mainly convergent while for the other BP the pattern is divergent along the radial OZ direction and convergent along the others. Here also, this visual analysis is confirmed by using the application "divergence" supplied by OOMMF. However, the spatial distribution of the three-dimensional magnetization vector field is a little bit more difficult to explore for the dot ($116 \times 50 \times 200$ nm^3) as the vortex line is not along a straight line strictly parallel to OZ as in the wire's case but slightly tilted, so that the vortex core ends at both extremities (planes $z = 0$ and $z = 40$ nm) at different levels: $\Delta y = 4$ nm.

To describe the remagnetization of the structure, the same experimental procedure was used as before in the

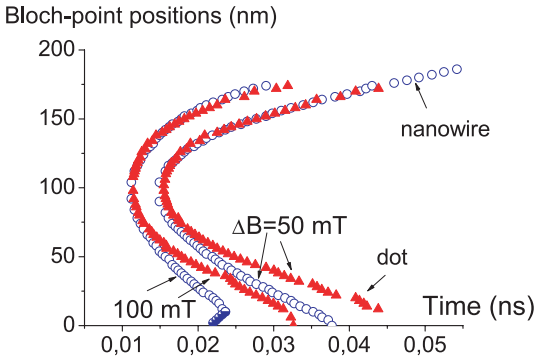

Fig. 14. Evolution with time of the position of the pair of Bloch-points versus ΔB for the dot geometry ▲ and wire one (◯). Width $L_2 = 200$ nm.

L_1 case. Starting with the initial equilibrium magnetization obtained for the magnetic field just before inversion: $B = -289$ mT (-378 mT) for dot (and nanowire) respectively, different calculations were performed with a constant reversal field. In the numerical experiments, the increase of the amplitude of the applied field was in the range from 50 to 200 mT (i.e. from $B = -339$ mT to -489 mT for the dot). The positions of the two Bloch points situated at the extremities of the reversed segment were collected and are reported as function of time in Figure 14 for different values of the field increment ΔB.

The time t_1 needed for the appearance of the magnetization reversal process approximately follows the relation: $t_1 \approx 0.1/\sqrt{\Delta B}$ both for dot and nanowire (with t_1 in ns and ΔB in mT). Note that this expression is quite similar to that expressed for the nucleation of a single point in the previous case where $L = 40$ nm. At the very beginning, Bloch-points move quite fast. This motion slows down with increasing time. However, a huge difference is noticeable between the mobility of the two Bloch points and between the different geometries studied. Moreover, for a high ΔB value a secondary nucleation of a single Bloch point from the surface $z = 200$ nm may occur. An overall average value of Bloch-point velocity has been calculated when the reversed segment length increases from 60 to 120 nm. One obtains a linear relation of the type $V_{BP} = v_o + \mu \Delta B$. A large discrepancy is noticeable between the two geometries. The BP mobility amounts to $\mu = 0.025$ m/s mT for the dot and reaches a much higher value for the nanowire: $\mu = 0.095$ km/s mT. Furthermore, in the case of a nanowire the two Bloch-points behave quite differently along the line. The first BP moves quickly towards the surface $z = 0$. It is useful to recall here that near this surface and due to precession effects, the moments acquire a larger radial component. Such an effect is less pronounced in the case of dot. However the motion of the second Bloch point towards the surface $z = 200$ nm is much slower whatever the geometry studied. Finally, similar as for shorter stripes of length L_1, the velocity does not tend to zero with ΔB. Although BP injection is locked by an energy barrier, artificial injection of one BP near a surface or a pair of BP in the middle of the core line, even below the critical field amplitude, leads to a full reversal of the chirality of the wall.

7 Conclusion

We have investigated the magnetization reversal of three different elements: an infinite thin film, a wire and an isolated dot. All of them are able to support stripe domains in the remanent state. Various codes were used according to the geometry studied. While the nucleation of domains, in an infinite slab, is a continuous process occurring over the whole sample area, we have shown that for wires and dots in decreasing field, the magnetization starts to oscillate in the vicinity of surfaces at both ends of the element only. However, the preliminary results show that the developing stripe pattern is strongly affected by the numerical protocol followed in particular the method of decreasing the applied field (large or small steps). In all cases, this implies a tiny step in the $M(B)$ curve. On the other hand, taking advantage that standard micromagnetic calculations involving Bloch points are less problematic than it might seem, we presented in this paper the study of the main hysteresis loop for these three geometries. For wires and dots only, and according to the width of the stripes, we showed that the inner wall polarity reversal is induced either by nucleation of an isolated BP near one surface (short width) or via a pair of BP in the middle of the line for larger width. A description of the different magnetization distributions of BP has been shown and tentatively proposed. A description of the key characteristics of the BP displacements are presented and discussed in detail. Several problems need to be clarified experimentally. The first one is linked to the field variation of the period of the pattern. Calculations predict a huge effect, in particular near the reversal field. It would be worthwhile to follow the evolution of W with B for a thin slab while at each step of the observation a small AC field of decreasing amplitude is applied in order to attempt the lowest energy configuration, including an adjustment of the number of stripes. For elements of finite size, it would be interesting to follow the stripe formation and see how this magnetic pattern invades the whole volume. Last but not least would be the observation of the core reversal of the inner wall of the stripe under field. While direct experimental proofs of the existence of BP's have been clearly established for Garnet films [30,31], it would be interesting to undertake similar experiments for metallic thin films and dots.

The authors are very grateful to Dr. Yves Roussigné for enlightening and stimulating discussions on this subject, to Pr. J. Linarès and Dr. L. Thomas for fruitful discussions and numerical help and to Dr. S. Thompson for a critical reading of the manuscript.

References

1. G. Prinz, Science **282**, 1660 (1998)
2. A. Hubert, R. Schäfer, *Magnetic Domains* (Springer-Verlag, Berlin, 1998)

3. M.W. Muller, Phys. Rev. **122**, 1485 (1961)
4. R. Ferré, M. Hehn, K. Ounadjela, J. Magn. Magn. Mater. **165**, 9 (1997)
5. M. Labrune, J. Miltat, J. Appl. Phys. **75**, 2156 (1994)
6. Y. Nakatani, N. Hayashi, IEEE Trans. Magn. **24**, 3039 (1988)
7. Y. Nakatani, N. Hayashi, IEEE Trans. Magn. **29**, 2587 (1993)
8. A. Thiaville, J.M. Garcia, R. Dittrich, J. Miltat, T. Schrefl, Phys. Rev. B **67**, 094410 (2003)
9. R. Hertel, J. Kirschner, J. Magn. Magn. Mater. **278**, L291 (2004)
10. N. Vukadinovic, O. Vacus, M. Labrune, O. Acher, D. Pain, Phys. Rev. Lett. **85**, 2817 (2000)
11. P. Trouilloud, J. Miltat, J. Magn. Magn. Mater. **66**, 99 (1987)
12. LLG Micromagnetic simulator^{TM} `http://llgmicro.home.mindspring.com/`
13. OOMMF was developped by M.J. Donahue, D. Porter from NIST. See `http://math.nist.gov/oommf`. 3rd version of the 1.2a3 release
14. M. Hehn, S. Padovani, K. Ounadjela, J.P. Bucher, Phys. Rev. B **54,** 3428 (1996)
15. M. Labrune, H. Niedoba, Eur. Phys. J. B **27**, 103 (2002)
16. N. Saito, H. Fujiwara, Y. Sugita, J. Phys. Soc. Jpn. **19**, 1116 (1964)
17. D. Pain, Ph.D. Thesis, University of Versailles (1999)
18. D. Billet, private communication, MFM observations of stripe pattern under an in-plane applied field
19. G. Suran, M. Naili, H. Niedoba, F. Machizaud, O. Acher, D. Pain, J. Magn. Magn. Mater. **192**, 443 (1999)
20. S. Foss, C. Merton, R. Proksch, G. Skidmore, J. Schmidt, E.D. Dahlberg, T. Pokhil, Y-T Cheng, J. Magn. Magn. Mater. **190**, 60 (1998)
21. M.E. Schabes, H.N. Bertram, J. Appl. Phys. **64,** 1347 (1988)
22. R.P. Cowburn, J. Phys. D **33** (2000)
23. M. Hehn, R. Ferré, K. Ounadjela, J.P. Bucher, F. Rousseaux, J. Magn. Magn. Mater. **165**, 5 (1997)
24. I.L. Prejbeanu, L.D. Buda, U. Ebels, M. Viret, C. Fermon, K. Ounadjela, IEEE Trans. Mag. **37**(4), 2108 (2001)
25. W. Brückner, J. Thomas, R. Hertel, R. Schäfer, C.M. Schneider, J. Magn. Magn. Mater. **283**, 82 (2004)
26. E. Feldkeller, Z. Angew. Phys. **19**, 530 (1965)
27. M. Kléman, *Points, Lines and Walls* (Wiley, Chichester, 1983)
28. P.R. Kotiuga, IEEE. Trans. Magn. **25**, 3476 (1989)
29. J.C. Slonczewski, A.P. Malozemoff, *Physics of domain walls in magnetic garnet films*, International School of Physics – Varenna Italy June/July 1977 (Physics of Magnetic Garnets, Soc. Italiana di Fisica – Bologna, Italy, 1978)
30. Y. Kabanov, L. Dedukh, V. Nikitenko, Pis'ma Zh. Eksp. Teor. Fiz. **49**, 551 (1989); Y. Kabanov, L. Dedukh, V. Nikitenko, JETP Lett. **49**, 637 (1989)
31. A. Thiaville, J. Miltat, Europhys. Lett. **26**, 1006 (1994)